ELSEVIER

Surface Science 402–404 (1998) 351–355

surface science

Mechanical stress and magnetism of ferromagnetic monolayers

D. Sander *, A. Enders, C. Schmidthals, D. Reuter, J. Kirschner

Max-Planck-Institut für Mikrostrukturphysik, Weinberg 2, D-06120 Halle, Germany

Received 4 July 1997; accepted for publication 3 October 1997

Abstract

A combination of in-situ stress measurements with low-energy electron diffraction and scanning tunneling microscopy is used to investigate structural transitions during film growth. The formation of misfit distortions during the growth of Fe on W(110) and the formation of different coincidence structures for the growth of Ni on W(110) are identified with high sensitivity by characteristic changes in the stress versus coverage curves. The influence of structural changes on the magnetic properties of Fe films is examined with magneto-optical Kerr effect measurements. © 1998 Elsevier Science B.V. All rights reserved.

Keywords: Epitaxy; Iron; Low energy electron diffraction; Magneto-optical Kerr effect; Nickel; Scanning tunneling microscopy; Stress measurements; Tungsten

1. Introduction

The growth and structure of the ferromagnetic 3d elements Fe, Co and Ni on W(110) have been studied extensively by low-energy electron diffraction (LEED) [1–9] and scanning tunneling microscopy (STM) [10–14]. These structural investigations show that Fe, Co and Ni grow pseudomorphically on W(110) for small coverages in the submonolayer range. However, as a result of the considerable lattice mismatch of these elements with respect to tungsten, in the monolayer range structural transitions like the formation of misfit distortions or the formation of coincidence structures are observed by LEED and STM and will be discussed with respect to film stress for the growth of Fe and Ni on W(110). Our in-situ stress measurements provide experimental evidence for the concept of strain as a driving force for structural transitions in monolayer films. These structural transitions induce characteristic changes of the magnetic properties. In-situ magneto-optical Kerr effect measurements reveal a considerably increased coercivity for sesquilayer Fe films and in-plane reorientation of the easy axis of magnetization of Stranski–Krastanov Fe layers.

2. Stress measurement

We use a simple optical deflection technique to measure film stress with submonolayer sensitivity [15] by monitoring the bending of a 0.1 mm thick W(110) crystal (length 13 mm along W[001], width 3 mm along W[$\bar{1}$10]) during film growth on the front side of the substrate, which is clamped at its top end along the width to a sample manipulator. The film stress on the front side induces a minute bending of the substrate with a radius of

* Corresponding author. Fax: (+49) 345 5511223; e-mail: sander@mpi-halle.mpg.de

PII: S0039-6028(97)00922-9

curvature of the order of 1 km. Thus, the curvature of the thin crystal is a measure for the stress acting in the film. We measure the growth-induced change of the radius of curvature of the crystal along W[001], and derive the corresponding change of the stress state in the film–substrate composite [15,16]. Note that it is not only the film stress due to lattice mismatch which can induce a bending of the substrate, but also differences in the surface stress of the clean substrate versus the substrate–film composite.

The film materials were deposited by electron-beam evaporation from high-purity wires. Growth rates of the order of 0.1 nm min^{-1} were calibrated with a quartz oscillator. We define a coverage of one monolayer (ML) as an atomic aerial density of 1.41×10^{15} cm^{-2} for Fe and 1.82×10^{15} cm^{-2} for Ni.

3. Stress and structure of Fe and Ni monolayers

Pseudomorphic growth of Fe on W(110) for coverages of up to 1.5 ML was found in LEED and STM investigations [1,10–14]. Thus, the large lattice mismatch between Fe ($a_{Fe} = 2.87$ Å) and W ($a_W = 3.17$ Å) of almost 10% is expected to induce considerable tensile strain in the pseudomorphic growth regime. In contrast to the tensile stress expected from strain arguments, our stress measurement (Fig. 1a) reveals compressive stress for submonolayer coverages of up to 0.6 ML. The compressive stress measured in the submonolayer range for different growth temperatures and also for Ni (Fig. 1a–c) clearly indicates the dominant surface stress contribution to the adsorbate-induced bending of the crystal [17]. Our stress measurements suggest that the tensile strain expected for pseudomorphic Fe, Co and Ni submonolayer coverages does not necessarily induce tensile stress. Only for larger film coverages (above half a monolayer film) can stress be qualitatively described by strain arguments. For Fe, a tremendous tensile stress of the order of 3 N m^{-1} per ML ($\sim$20 GPa) sets in above 0.6 ML. This order of tensile stress is expected from lattice mismatch arguments [14]. We ascribe the kink of the stress curve at 1.5 ML to the onset of the formation of misfit distortions in the growing film. As a result, the stress increase is considerably reduced after the introduction of misfit distortions. Gradmann and Waller [1] described satellites in LEED emerging for coverages above 1.7 ML, which were ascribed to misfit distortions along W[$\bar{1}$10]. Starting from 3 ML, LEED shows the characteristic distortion pattern of Fig. 2a, first discussed in Ref. [1]. The clear appearance of extra diffraction spots indicates a highly ordered distortion line network, a real-space image of which is presented in the STM image of Fig. 2b, recently also described by Bethge

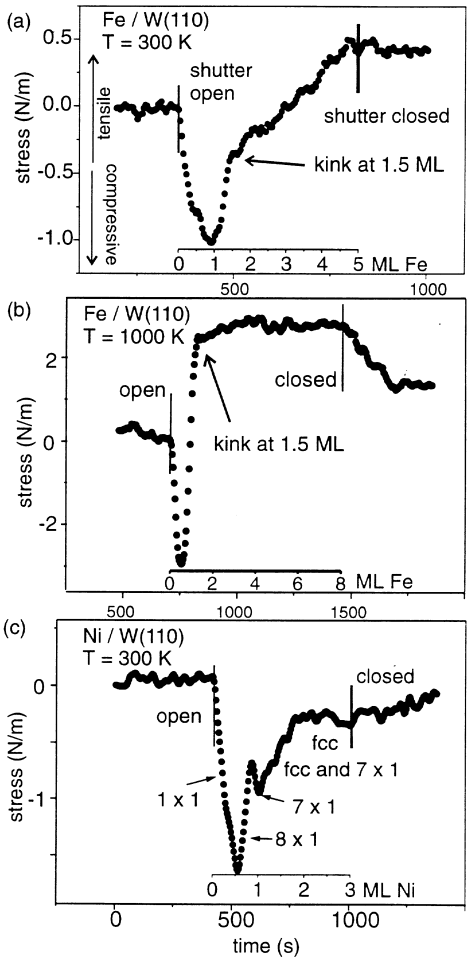

Fig. 1. In-situ film stress measurements. (a) Growth of 5 ML Fe at 300 K. (b) Growth of 8 ML Fe at 1000 K. (c) Growth of 3 ML Ni at 300 K. The different Ni surface structures as obtained from LEED are indicated.

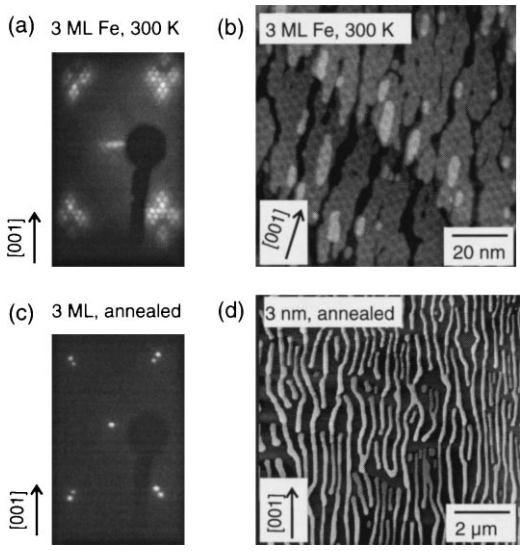

Fig. 2. (a) LEED of 3 ML Fe grown at 300 K: extra spots indicate a regular distortion line network, as shown in (b). (b) STM of 3 ML Fe grown at 300 K: elongated islands of the third layer (grey) and patches of the fourth layer on top of the third (lighter grey) show a hexagonal arrangement of distortion lines (dark lines) on the surface. (c) After annealing to 700 K, (a) transforms into a double diffraction pattern. (d) After annealing a 3 nm thick Fe film deposited at 300 K, STM shows elongated islands with a height of 17 nm.

et al. [12]. The formation of misfit distortions is a thermally activated process, and only for high-temperature Fe growth at 1000 K do we observe film growth practically free of stress, as indicated by the horizontal section of the stress curve of Fig. 1b. Note that the stress does not increase any further after the kink of the curve at 1.5 ML, although six more monolayers are deposited. Thus, at high temperatures the stress relief mechanism due to the formation of misfit distortions is much more efficient. After termination of growth, a partial stress relief is observed at 1000 K, leading to a final film stress close to that obtained for 1 ML Fe. Thus, only the first monolayer contributes to the film stress. Scanning Auger microscopy proved [18] that Stranski–Krastanov layers are formed for high-temperature growth. They are composed of Fe coalesced into islands which grow on top of the first pseudomorphic Fe monolayer. Consequently, Fig. 2c reveals a double diffraction pattern, characteristic of two bcc (110) unit cells, one of the pseudomorphically strained first monolayer and one of the relaxed Fe from the top of the islands. Fig. 2d reveals elongated islands along W[001], with an increased height of 17 nm with respect to the deposited amount of 3 nm. The reduction of the strain energy is proposed to be the main driving force for the island formation for two reasons: (i) the number of misfit distortions is reduced due to the much smaller size of the cross-sectional area of the island compared to the homogeneously covered first layer for layer-by-layer growth, and (ii) the final film stress after completion of growth is limited to the first layer, whereas for layer-by-layer growth, all layers contribute to the film stress.

Before we discuss the effect of the aforementioned structural transitions on the magnetism of the Fe layers, we present stress measurements on the growth of Ni on W(110) to show that even more subtle structural changes like the transition from a (8×1) to a (7×1) LEED coincidence structure are easily detected in a stress measurement. The growth of Ni on W(110) first leads to a (1×1) pseudomorphic phase, then to a (8×1) coincidence structure, followed by a (7×1) coincidence structure which indicates completion of the first monolayer. Further deposition produces an almost fcc (111)-like structure in the second layer with some residual strain. The third layer is found to grow essentially fcc (111)-like. A detailed description of the Ni monolayer structure can be found elsewhere [19]. In the Nishiyama–Wassermann growth mode observed by LEED [4,19] the Ni[$\bar{1}$10] direction of fcc Ni(111) is oriented parallel to W[001]. Assuming the validity of bulk atomic distances for Ni, a tensile strain of $\sqrt{2}a_{\mathrm{W}}/a_{\mathrm{Ni}}-1=27\%$ results along W[001] ($a_{\mathrm{W}}=3.17$ Å, $a_{\mathrm{Ni}}=3.52$ Å). However, our stress curve of Fig. 1c again indicates compressive stress in the submonolayer range where, based on lattice mismatch, tensile stress was expected. As in the case of Fe, only for coverages above half a monolayer can the stress curve be described, at least qualitatively, in view of the strain state of the film. The tensile stress measured during the formation of the (8×1) structure can be rationalized by

a tensile strain of 13% of that structure [17]. The subsequent formation of the (7×1) structure induces compressive stress, as expected from the slight compressive strain of -1.3% resulting from the higher areal density of this coincidence structure. Thus, the occurrence of the second minimum of the stress curve can be correlated with the completion of the first monolayer with a mainly (7×1) structure. In the perpendicular in-plane direction (W[$\bar{1}$10]), the strain remains constant at 3.7% for the completion of the first Ni monolayer [19]. Similar structural changes were observed for the growth of Co on W(110) [9] and led to similar changes in the stress curve [20].

4. Magnetism of Fe monolayers

The high coercivity of the sesquilayer Fe film and the in-plane reorientation of the easy axis of magnetization of Stranski–Krastanov layers corroborate the interplay between film structure and magnetism. The hysteresis loop of Fig. 3a shows a strong coercivity of the order of 0.2 T at 190 K for 1.5 ML Fe. Films of slightly lower and higher thickness show a moderate coercivity of well below 0.1 T at 140 K. We ascribe the high coercivity mainly to a strong pinning of the domain-wall movement due to the increased domain-wall energy in the islands of the second layer compared to the wall energy in the surrounding one monolayer thick film. The dimensions of the islands in the second layer, of the order of $5\,\text{nm}\times10\,\text{nm}$, as shown in the STM image of Fig. 3b, are sufficient to cause a strong pinning of the domain wall movement [14]. The easy axis of magnetization in the islands of the Stranski–Krastanov layers shown in Fig. 2d is reoriented to [001], as deduced from the MOKE curves of Fig. 3c. Whereas the rectangular-shaped hysteresis loop of the transversal Kerr geometry indicates an easy axis of magnetization along [$\bar{1}$10], after annealing the same geometry leads to a hard axis loop. Now the easy axis magnetization curve is observed in the longitudinal geometry, indicating a reoriented direction of the easy axis from [$\bar{1}$10] to [001] in the annealed film. The slight curvature of the polar magnetization

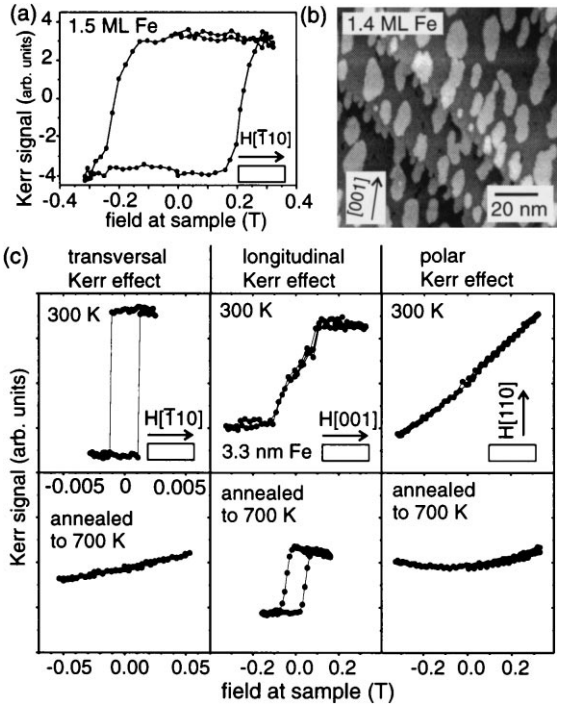

Fig. 3. MOKE of Fe monolayers grown at 300 K. (a) High coercivity of 0.2 T at 190 K of the sesquilayer 1.5 ML film, shown in the STM image. (b) Lighter grey patches of the second layer sit on top of the homogeneously covered first Fe layer (darker grey). (c) MOKE of 3 nm Fe deposited at 300 K (upper row), and after annealing to 700 K (lower row). The easy axis switches from [$\bar{1}$10] to [001] due to annealing.

curve of the annealed film is ascribed to a quadratic Voigt effect of the UHV window. The effective anisotropy against perpendicular magnetization increased for the annealed film, as shown in the almost negligible polar magnetization in fields of up to 0.4 T in the polar geometry. The maximum height of the Fe islands of 17 nm obtained from the STM image of Fig. 2d indicates a locally increased Fe thickness compared to the nominally deposited amount. Whereas for room-temperature growth of Fe on W(110), the in-plane reorientation of the easy axis from [$\bar{1}$10] to [001] was observed for thicknesses of the order of 10 nm [21], our Stranski–Krastanov layers show this reorientation of the easy axis for much smaller depositions due to the coalescence of the deposited Fe into islands.

Acknowledgements

We acknowledge enlightening discussions with U. Gradmann on the magnetism of sesquilayer Fe films.

References

[1] U. Gradmann, G. Waller, Surf. Sci. 116 (1982) 539.
[2] P.J. Berlowitz, J.W. He, D.W. Goodman, Surf. Sci. 231 (1990) 315.
[3] T.U. Nahm, R. Gomer, Surf. Sci. 337 (1997) 237.
[4] J. Kolaczkiewicz, E. Bauer, Surf. Sci. 144 (1984) 495.
[5] K.P. Kämper, W. Schmitt, G. Güntherodt, H. Kuhlenbeck, Phys. Rev. B 38 (1988) 9451.
[6] J.E. Whitten, R. Gomer, Surf. Sci. 316 (1994) 1.
[7] J.E. Whitten, R. Gomer, Surf. Sci. 316 (1994) 22.
[8] J.E. Whitten, R. Gomer, Surf. Sci. 316 (1994) 36.
[9] H. Fritzsche, J. Kohlhepp, U. Gradmann, Phys. Rev. B 51 (1995) 15933.
[10] H.J. Elmers, J. Hauschild, H. Höche, U. Gradmann, H. Bethge, D. Heuer, U. Köhler, Phys. Rev. Lett. 73 (1994) 898.
[11] H.J. Elmers, J. Hauschild, J. Fritzsche, G. Liu, U. Gradmann, U. Köhler, Phys. Rev. Lett. 75 (1995) 2031.
[12] H. Bethge, D. Heuer, Ch. Jensen, K. Reshöft, U. Köhler, Surf. Sci. 331–333 (1995) 878.
[13] M. Bode, R. Pascal, M. Dreyer, R. Wiesendanger, Phys. Rev. B 54 (1996) R8385.
[14] D. Sander, R. Skomski, C. Schmidthals, A. Enders, J. Kirschner, Phys. Rev. Lett. 77 (1996) 2566.
[15] D. Sander, A. Enders, J. Kirschner, Rev. Sci. Instrum. 66 (1995) 4734.
[16] H. Ibach, C.E. Bach, M. Giesen, A. Grossmann, Surf. Sci. 375 (1997) 107.
[17] D. Sander, C. Schmidthals, A. Enders, J. Kirschner, Phys. Rev. B. 57 (1998) 1406.
[18] D. Reuter, G. Gerth, J. Kirschner, in: M.C. Tringides (Ed.), Surface Diffusion: Atomistic and Collective Processes, Plenum, New York, 1996, p. 489.
[19] C. Schmidthals, A. Enders, D. Sander, J. Kirschner, Surf. Sci., this issue.
[20] A. Enders, D. Sander, J. Kirschner, Verhdl. DPG (VI) 32 (1997) O7.4.
[21] U. Gradmann, J. Korecki, G. Waller, Appl. Phys. A 39 (1986) 101.